Sustainable Energy & Fuels

ROYAL SOCIETY OF CHEMISTRY

PAPER

View Article Online
View Journal | View Issue

Check for updates

Cite this: *Sustainable Energy Fuels*, 2025, **9**, 3820

Experimental study on hydrogen-rich fuel generation *via* ammonia decomposition using a structured catalytic reactor†

Payam Shafie, *[a] Marie Mottoul,[b] Alain DeChamplain[a] and Julien Lepine[c]

Thermo-catalytic ammonia decomposition has gained significant attention for its ability to produce a CO_x-free H_2-rich fuel. Due to the scalability advantages of structured reactors, this study experimentally evaluates the efficiency of a non-commercial stainless-steel monolithic Ru/Al_2O_3 catalyst to determine operating conditions for achieving practical partial conversion rates for applications such as dual-fuel engines. The analysis focuses on the effects of residence time and temperature on ammonia conversion, the heating value of H_2-rich gas, and the thermal energy required. The results show that higher temperatures and longer residence times significantly improve ammonia conversion, with conversion nearing completion observed at 600 °C and a flow rate of 50 mL min^{-1}. However, due to the low Ru loading on the monolith surface, ammonia conversion at 400 °C remained limited to 12%. Kinetic analyses revealed that achieving practical conversion rates above 60% with the catalytic reactor requires extending the residence time to 85 s at 500 °C. Additionally, supplying 50% of the input energy for a 200 kW dual-fuel engine using H_2-rich fuel would require only 37% of the available exhaust energy to meet the heating demand for ammonia decomposition at 400 °C with a 60% conversion rate. To further enhance the reactor's performance and scalability, targeted improvements such as optimizing catalyst loading, incorporating promoters, employing bimetallic Ru-based catalysts, refining reactor volume, and utilizing a parallel reactor configuration, could be explored to maximize efficiency and integration with practical energy systems.

Received 2nd May 2025
Accepted 21st May 2025

DOI: 10.1039/d5se00626k

rsc.li/sustainable-energy

Open Access Article. Published on 28 de maig 2025. Downloaded on 1/2/2026 10:54:36.
This article is licensed under a Creative Commons Attribution-NonCommercial 3.0 Unported Licence.

1. Introduction

The clean, zero-carbon nature of hydrogen, combined with its high energy density, diverse production methods, and environmentally friendly generation and utilization processes, has prompted many governments to recognize it as a key component of the energy transition.[1] With the rapid advancement of policy frameworks and hydrogen energy technologies, the applications of hydrogen energy are expanding across various sectors, including energy storage, fuel, transportation, and steel metallurgy, with its usage expected to become even more widespread.

However, the storage and transportation of hydrogen remain a key drawback due to its high-pressure gaseous and low-temperature liquid storage as its common physical storage methods.[2] As an example regarding the safety, in 2019, three hydrogen explosion accidents caused by H_2 tank leakage were reported in Norway and South Korea, amplifying the public's concerns about the diffusibility, inflammability, explosibility, and intrinsic safety of hydrogen.[3] As well as the high energy consumption and safety issues, such storage and transportation systems account for approximately 30% of the overall cost of hydrogen, which is currently exorbitant and significantly higher than traditional fuels, such as natural gas.[4] Consequently, in order to bypass the bottleneck in the hydrogen industry, it is extremely important to develop hydrogen storage and transportation technology that is safe, commercially available, and efficient.

To address these challenges, ammonia (NH_3) has gained recognition as a highly promising hydrogen carrier, due to its high hydrogen density (120 kg_{H_2} m^{-3}) and higher boiling point (−33 °C).[5] Moreover, with a global production capacity of 236 million tonnes in 2021, the existing infrastructure for ammonia storage and transportation is well-established due to the ease of liquefaction and using regular stainless-steel pipes and containers.[6,7] Furthermore, ammonia enables the repurposing of various existing fossil fuel infrastructure components, such as liquefied natural gas (LNG) terminals, liquefied petroleum gas (LPG) refueling stations, and retrofitted internal combustion engines. Such advantages can be attributed to its broad range of applications such as a fuel, hydrogen carrier, fertilizer, chemical intermediate, and refrigerant.[8]

[a]*Department of Mechanical Engineering, Laval University, Quebec, Canada. E-mail: payam.shafie.1@ulaval.ca*

[b]*Department of Chemical Engineering, Laval University, Quebec, Canada*

[c]*Department of Operations and Decision Systems, Laval University, Quebec, Canada*

† Electronic supplementary information (ESI) available. See DOI: https://doi.org/10.1039/d5se00626k

This journal is © The Royal Society of Chemistry 2025

Open Access Article. Published on 28 de maig 2025. Downloaded on 1/2/2026 10:54:36.
This article is licensed under a Creative Commons Attribution-NonCommercial 3.0 Unported Licence.

Ammonia combustion presents several limitations, mainly due to its inherently slow flame propagation compared to other fuels. Additionally, its combustion process leads to the release of nitrogen-based emissions, which can contribute to environmental concerns. To overcome these limitations and enhance combustion efficiency, one effective approach is to use ammonia as a hydrogen carrier. By breaking it down just before use, a H_2-rich fuel can be generated, improving its reactivity while simplifying its handling.[9,10] Therefore, thermal catalytic decomposition of ammonia has attracted considerable interest due to its capability to generate an on-demand, CO_x and sulfur-free hydrogen stream, making it suitable for applications such as engines, fuel cells, turbines, and industrial furnaces.[11]

South Korea, Japan, the USA, and Australia are leading the development of various ammonia decomposition systems aimed at hydrogen production for multiple sectors. For instance, POSCO Holdings in South Korea, plans to establish a hydrogen production plant through ammonia decomposition with a target capacity of 1000 m^3 h^{-1} by 2025.[12] Canada is among the top ten countries in the world for ammonia production, with an annual production of approximately 5 million tonnes. Additionally, advancements in carbon capture technology have facilitated the production of blue ammonia, while water electrolysis powered by renewable energy enables the generation of green ammonia.[13] This readily available resource positions the country as a potential hub for the development of hydrogen production through ammonia decomposition. Therefore, one of the motivations for this study is that despite the growing global interest in ammonia as a hydrogen carrier and its critical role in power infrastructures such as marine applications, there remains gaps in the Canadian research landscape especially in exploring the practical implementation of ammonia decomposition as a hydrogen production pathway.

The endothermic decomposition of ammonia is the reverse of its synthesis so that it requires less than a quarter of the energy needed for water splitting and roughly a fifth less than steam methane reforming.[14] Furthermore, the lower operating temperature required for ammonia decomposition compared to steam methane reforming, enhances catalyst longevity and hydrogen production efficiency, while also eliminating the issue of carbon emission.[15] From a theoretical perspective, elevated pressures are unfavorable for ammonia decomposition, and the reaction is best carried out at low atmospheric pressures.[16] While ammonia decomposition can occur with or without a catalyst, using a proper catalyst can lower the required temperature for an efficient reaction. Although the reaction is reversible, the catalysts that proved most effective for ammonia synthesis were not necessarily the most efficient for its decomposition. Therefore, catalysts are being developed to facilitate ammonia decomposition at lower temperatures while achieving high conversion rates.[15,16] By evaluating various catalysts supported on alumina, researchers determined the relative activity for ammonia decomposition as follows: Ru > Ir > Rh > Ni > Pt > Pd > Fe.[17] However, since the choice of support could also influence catalytic performance, the relative activity order may vary with other supports. For example, in the study by Yin *et al.*,[18] at a reaction temperature of 400 °C, ammonia conversion rate for catalysts supported on carbon nanotubes (CNT) followed the order: Ru > Ni > Pd > Fe.

Most recent studies on ammonia decomposition have focused on the development of catalyst in the form of powder and fixed-bed reactors.[19] Ni-based catalysts are considered non-precious metal alternatives, and their catalytic performance is highly dependent on the particle size.[17] The study conducted by Zhang *et al.*[20] showed that the particle sizes below 5 nm exhibit a significant enhancement in catalytic performance, but at temperatures above 400 °C, there is a concern of particle agglomeration leading to larger particle sizes. The addition of rare metal promoters is considered to have a beneficial effect on improving the catalytic performance of Ni. Okura *et al.*[21] showed that using Gd as the promoter can increase the ammonia decomposition rate by a factor of 1.2. Chein *et al.*[22] conducted a numerical study using a one-dimensional model to analyze ammonia decomposition in a cylindrical fixed-bed reactor involved a Ni–Pt/Al_2O_3 catalyst bed operating under atmospheric pressure. The study indicated that the reactor achieved NH_3 conversion rates exceeding 99% at temperatures above 600 °C, particularly when operating at low ammonia flow rates (below 10 mL min^{-1}). Regarding Ru-based catalysts, Devkota *et al.*[23] theoretically simulated a large-scale hydrogen plant with a single or multi-catalytic Ru fixed beds for ammonia decomposition including Temperature Swing Adsorbers (TSA) and Pressure Swing Adsorbers (PSA) for purification of hydrogen. They concluded that the single-bed reactor had a maximum conversion rate of nearly 35%, while the combination of multi-bed reactor in series, reached an almost equilibrium conversion of 97%. Cha *et al.*[24] investigated the combination of catalytic ammonia decomposition using Ru catalyst in a fixed-bed reactor by a 1 kW fuel cell. They showed that by maintaining the temperature at 550 °C, a conversion rate of about 99.8% and a maximum overall efficiency of 31% for the integrated system were achievable.

Fixed-bed reactors usually lead to a large pressure drop, temperature gradient and inconsistent flow.[25] On the other hand, structured reactors especially monolithic ones contain channels in a single block of inert or catalytic material, leading to low pressure drop, proper scale up, high surface area-to-volume ratio, enhanced mass transfer, and low weight.[26] Monolith catalysts also provide enhanced mechanical stability, which is crucial for high-temperature reactions like ammonia decomposition. This makes them a dependable option for long-term operations. As a result, over 100 000 m^3 of monolithic catalysts are manufactured globally each year for applications such as reducing engine emissions.[27] Plana *et al.*[28] showed that by using a honeycomb cordierite reactor and a Ni/Al_2O_3 catalyst, higher ammonia conversion rates were obtained compared to the same catalyst in a fixed bed reactor, due to better heat distribution and mass transfer. Moreover, Gyak *et al.*[29] conducted an experimental study on a ceramic-based monolith for ammonia decomposition utilizing a Ru/Al_2O_3 catalyst at 600 to 1000 °C. Their study demonstrated that at 700 °C and a low NH_3 inlet flow rate of 36 SCCM, nearly complete conversion was achieved. However, they highlighted the challenge of low decomposition rates at lower temperatures. Some of the challenges of structured reactors include difficult uniform loading of the catalyst onto the reactor structure and fouling over. One

Open Access Article. Published on 28 de maig 2025. Downloaded on 1/2/2026 10:54:36.
This article is licensed under a Creative Commons Attribution-NonCommercial 3.0 Unported Licence.

of the key challenges of structured reactors is the probability of non-uniform catalyst distribution on the reactor surface. Additionally, fouling over time can further impact reactor longevity and effectiveness.

Given the superior scalability of structured catalytic reactors for industrial applications, as well as the potential waste heat recovery integration, this study aims to provide a scientific contribution by experimentally investigating thermal ammonia decomposition. The research integrates a non-commercial stainless-steel monolith-based Ru/Al_2O_3 catalyst, a dual-layer vacuum cold trap for efficient removal of unreacted NH_3, and a continuous, cost-effective hydrogen sensor. The primary focus is on assessing the impact of the residence time and reaction temperature on the reactor performance. Moreover, this setup enables accurate hydrogen measurement while addressing key challenges such as NH_3 corrosivity and real-time monitoring, all within a compact and economical configuration. By evaluating factors such as steady-state time, conversion rate, H_2-rich gas heating value, and required heating power, the findings will support the development of more efficient hydrogen production systems. Additionally, the characteristics of a sample dual-fuel engine are analyzed to estimate real-scale residence time and heating energy requirements, providing insights for potential future waste-energy based applications.

2. Methodology and experimental test rig

The mechanism considered for the decomposition of ammonia involves a series of steps commencing with the adsorption of NH_3 molecules onto the catalyst surface ($NH_{3(a)}$ generation), followed by dehydrogenation processes ($N_{(a)}$ and $H_{(a)}$ generation), and ultimately, the desorption of hydrogen and nitrogen atoms into gaseous H_2 and N_2:[30]

$$NH_{3(g)} + * \rightleftarrows NH_{3(a)} \quad (1)$$

$$NH_{3(a)} + * \rightleftarrows NH_{2(a)} + H_{(a)} \quad (2)$$

$$NH_{2(a)} + \rightleftarrows NH_{(a)} + H_{(a)} \quad (3)$$

$$NH_{(a)} + * \rightleftarrows N_{(a)} + H_{(a)} \quad (4)$$

$$2N_{(a)} \rightleftarrows N_{2(g)} + 2* \quad (5)$$

$$2H_{(a)} \rightleftarrows H_{2(g)} + 2* \quad (6)$$

where the subscripts are as follows: (g) represents the gas state, (*) represents an empty site on the catalyst surface and (a) refers to a species adsorbed on the surface.

The catalytic performance of NH_3 decomposition varies significantly in terms of NH_3 conversion rate as the atomic activity is strongly influenced by morphologies and the number of active sites. The interaction of active sites on the metal catalyst with support materials can also play an important role in decomposing NH_3 into nitrogen and hydrogen, and in stabilizing unstable intermediate species like $N_{(a)}$ and $H_{(a)}$ through charge transfer between adsorbed sites on the catalyst surface and support. Ru-based catalysts are known to be more efficient due to the stabilized bond formation of Ru–N in reactions (4) and (5), preventing the desorption or recombination of $N_{(a)}$ into ammonia and ensuring the reaction proceeds efficiently toward full decomposition.[31]

Regarding the catalyst in this study, alumina serves as a high-surface-area support for Ru so that a 5 wt% Ru/Al_2O_3 catalyst is wash coated on the corrugated and flat stainless steel mesh substrates (as the structural support). The coated catalyst structure is then put through a heat treatment process in air to ensure proper adhesion and stabilisation on the catalyst structure before reduction. Then the catalyst mesh is rolled into a 19 mm × 100 mm cylindrical bundle with triangular channels to be used as a monolith reactor bed. Moreover, the catalyst is reduced by hydrogen at 300 °C to ensure the availability of clean and active Ru sites for the reaction. A quartz tube with dimensions of ID = 19 mm, OD = 26 mm and L = 615 mm including two reducer caps is utilized as the catalyst reactor. It is worth mentioning that the length of the heated zone of the tube furnace is 300 mm, which is much longer than the dimension of the catalyst bundle placed in the center of the tube furnace. So, it can be assumed that the temperature along the catalyst is uniform considering the uniformity profile of the furnace,

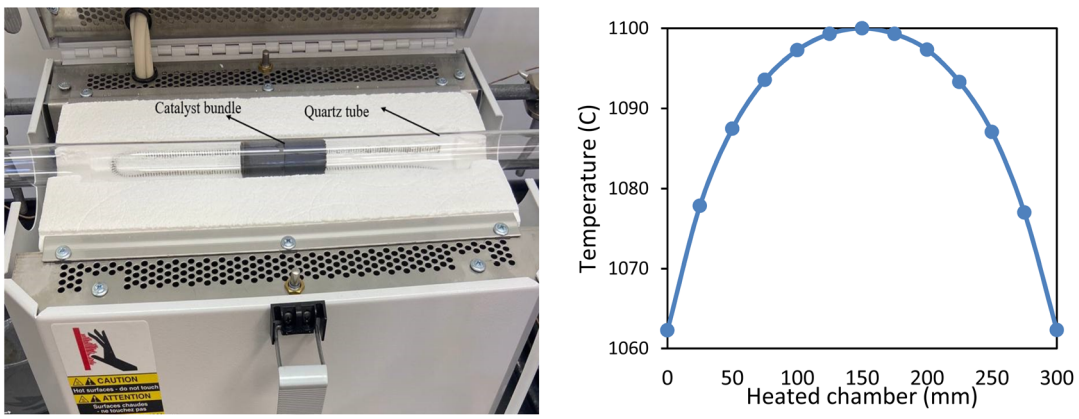

Fig. 1 Quartz tube and catalyst bundle position inside the tube furnace (left), uniformity of the furnace temperature based on data from the manufacturer.[32]

 This journal is © The Royal Society of Chemistry 2025

Open Access Article. Published on 28 de maig 2025. Downloaded on 1/2/2026 10:54:36.
This article is licensed under a Creative Commons Attribution-NonCommercial 3.0 Unported Licence.

which showed a maximum variation of only 0.45% at a distance of 50 mm from the center (Fig. 1).

The experimental setup includes the following parts (Fig. 2): liquid NH_3 storage tank (Linde, 99.999% purity, 7.86 bar), NH_3 single-stage regulator (0–3.5 bar with dip purge), N_2 tank for purging, pressure relief valve (Aquatrol, with the setpoint of 2 barA), mass flow controller (Alicat, 0–500 SCCM), tube furnace (Thermo Scientific, single zone, 800 W), cold trap for removing unreacted NH_3 (Jackhammer, dual-jacketed glass), water scrubber (2 L) to react with the possible remaining ammonia and remove it from the gas stream, drying column (Drierite, 200 L h^{-1}) to remove moisture of the stream, H_2 sensor (XEN-5320, 100 ppm-100%), and Bubble flow meter to measure the volumetric flow rate (Restek, 50 mL). Two thermocouples (Omega, K-type) are also used at the inlet and outlet of the reactor. Fig. 3 shows the ammonia decomposition test setup, put in place in this study.

Due to performing the purge before and after each test by N_2, it can be considered that the only products at the outlet of the reactor are H_2, N_2 and unreacted NH_3. After the reactor, the outlet stream passes through the cold trap, filled by a −70 °C cold bath of dry ice and ethanol, so the unreacted NH_3 can be condensed and removed from the stream safely. This prevents NH_3 to enter H_2 sensor or to leak into the hood considering its corrosivity and toxicity.

Ammonia gas is a colorless, toxic substance with a density lower than air and a pungent odor, making leaks easily detectable. It becomes lethal only when its concentration reaches 1000 times the detectable level.[33] Therefore, all the tests are performed under the ventilated laboratory hood (Fig. 3). Moreover, a NH_3 portable detector (RKI-SC-04 with an alarm set point of 25 ppm) is placed inside the hood during the tests to monitor any possible ammonia leakage.

Moreover, due to the safety limits and preventing the leakage in different tubing junctions especially with the quartz tube, the experimental tests were done at 1 barA. Two types of tubes including stainless steel and polytetrafluoroethylene (PTFE) are

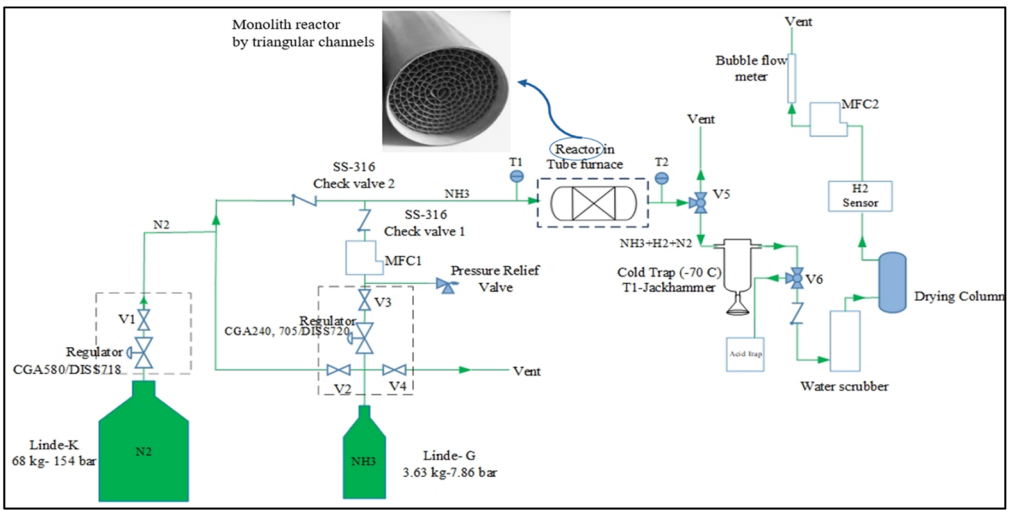

Fig. 2 Single-line diagram of the ammonia decomposition experimental setup including a schematic of a monolith cross section.

Fig. 3 Ammonia decomposition test setup.

Open Access Article. Published on 28 de maig 2025. Downloaded on 1/2/2026 10:54:36. This article is licensed under a Creative Commons Attribution-NonCommercial 3.0 Unported Licence.

used as well as using Swagelok valves and fittings. The acid trap, including a 2 M $H_2SO_4^-$ aqueous solution, is used during the final purge after each test to remove the condensed undecomposed NH_3 from the system through its neutralization by forming $(NH_4)_2SO4$ salt. The temperature monitoring by thermocouples indicates that for all test conditions, immediately before and after the reactor (less than 200 mm), the temperature was about 22 °C since the flow rate was very low. This also confirmed that after the regulator, gaseous ammonia enters the reactor.

Moreover, due to the fact that in some applications such as fuel cells, it is necessary to remove NH_3 before entering the fuel cell, using the cold trap demonstrates a possible strategy for recovering NH_3. Using such a compact H_2 sensor will be important in practical applications since it can work continuously (without the need for sampling) and it is much cheaper and smaller compared to some sophisticated analysers such as laser ammonia analysers which are 50–100 times more expensive.

3. Performance criteria

The experimental tests were conducted by varying two key parameters: the ammonia flow rate, which ranged from 50 to 300 SCCM, and the operating temperature of the furnace, which was tested at 400 °C, 500 °C, 550 °C, and 600 °C. Regarding the flow rate, a gas hourly space velocity (GHSV) is also defined as the number of reactor volumes that is fed at a specified condition which can be expressed per unit time (eqn (7)). Therefore, the higher the GHSV, the lower the residence time (τ).[34]

$$\mathrm{GHSV} = \frac{1}{\tau} = \frac{\dot{V}}{V} \tag{7}$$

where $\dot{V}$ ($m^3\ s^{-1}$) and V (m^3) are respectively standard volumetric gas flow rate and catalyst volume. Therefore, GHSV for different conditions of this study based on the volume of the reactor cylinder were 104, 208, 416 and 622 h^{-1}, which are equivalent to residence times of 35, 17, 8 and 6 s through the catalytic reactor.

Considering the definition of reduced pressure (P_R) and reduced temperature (T_R) based on eqn (8), and the fact that the compressibility factor (Z) is a function of P_R and T_R, Table 1 shows the compressibility factor for NH_3, H_2 and N_2 at 1 barA and 25 °C based on the experimental Z-factor table of Nelson–Obert.[35] Therefore, since the reduced pressures are less than 1 ($P_R \ll 1$) and the temperatures are higher than −173 °C, using ideal gas equation of state is a proper assumption for this study.

$$P_R = \frac{P}{P_{cr}}$$
$$T_R = \frac{T}{T_{cr}} \tag{8}$$

where P_{cr} and T_{cr} are the critical pressure and temperature. Eqn (9)–(11) are utilized for calculating the volumetric and mass concentrations of NH_3, H_2 and N_2.

$$M_{mix} = \sum y_i M_i \tag{9}$$

Table 1 Thermodynamic properties of gases at 1 barA and 25 °C (ref. 35)

	NH_3	H_2	N_2
M (kg $kmol^{-1}$)	17	2	28
T_{sat} (°C)	−33.3	−252.8	−195.8
T_{cr} (°C)	132.35	−239.85	−146.95
P_{cr} (bar)	112.8	13	33.9
T_R	0.76	9.25	2.44
P_R	0.01	0.08	0.03
Z	0.995	1	0.999

$$y_i = \frac{P_i}{P_{mix}} = \frac{V_i}{V_{mix}} = \frac{x_i/M_i}{\sum x_i/M_i} \tag{10}$$

$$P_{mix} = \frac{\rho R_u T}{M_{mix}} \tag{11}$$

where y_i, x_i, and M_i (kg $kmol^{-1}$) are the volumetric fraction, mass fraction and molar mass of each species in the mixture.

Ammonia conversion rate is determined using eqn (12), providing a direct measure of the efficiency of NH_3 decomposition.[34]

$$\mathrm{CR} = \frac{\dot{V}_{NH_3,\ reacted}}{\dot{V}_{NH_3,\ in}} \tag{12}$$

where $\dot{V}_{NH_{3,reacted}}$ and $\dot{V}_{NH_{3,in}}$ are the volumetric flow rates ($m^3\ s^{-1}$) of reacted ammonia at the outlet and the volumetric flow rate of ammonia at the inlet of the system. For each condition, once the hydrogen sensor reaches a steady state, the average volumetric flow rate during a minimum of 30 minutes is calculated and applied in eqn (12).

Considering the partial conversion of NH_3, the lower heating value (LHV) of the H_2-rich gas mixture (LHV_{mix}) is determined by considering the contributions of both hydrogen and unreacted ammonia in the reactor outlet stream (eqn (13)).[16]

$$\mathrm{LHV}_{mix} = \frac{\dot{m}_{H_2}\mathrm{LHV}_{H_2} + \dot{m}_{NH_3,\ out}\mathrm{LHV}_{NH_3}}{\dot{m}_{H_2} + \dot{m}_{NH_3,\ out}} \tag{13}$$

where $\dot{m}_{H_2}$ and $\dot{m}_{NH_{3,out}}$ represent the mass flow rates (kg s^{-1}) of hydrogen and unreacted ammonia at the reactor outlet, respectively, while LHV_{H_2} and LHV_{NH_3} correspond to their respective lower heating values. Moreover, the input energy required for the reaction (E_{in}) can be expressed as:

$$E_{in} = E_A + Q_h + Q_d \tag{14}$$

$$E_A = \dot{m}_{NH_{3,in}}\mathrm{LHV}_{NH_3} \tag{15}$$

$$Q_h = \dot{m}_{NH_{3,in}} C_P \Delta T \tag{16}$$

$$Q_d = \dot{m}_{NH_{2,in}} \Delta H_r \mathrm{CR}/M_{NH_3} \tag{17}$$

$$\mathrm{CP}(T) = \frac{R_u}{M_{NH_3}}\left(a_1 T^{-2} + a_2 T^{-1} + a_3 + a_4 T^1 + a_5 T^2 + a_5 T^3 + a_7 T^4\right) \tag{18}$$

 This journal is © The Royal Society of Chemistry 2025

Open Access Article. Published on 28 de maig 2025. Downloaded on 1/2/2026 10:54:36.
This article is licensed under a Creative Commons Attribution-NonCommercial 3.0 Unported Licence.

where Q_h (W) accounts for the heat necessary to raise the temperature of ammonia gas to the required reaction conditions and Q_d (W) is the heating energy needed for the ammonia decomposition at each conversion rate. The enthalpy change of the reaction (ΔH_r) is the difference between the enthalpy of the products at a specified state (H_P) and the enthalpy of the reactants at the same state (H_R) considering eqn (4)–(19) to (4)–(22).[35]

$$\Delta H_r = H_P - H_R \quad (19)$$

$$H_P = \Sigma N_p(\bar{h}_f^0 + \bar{h} - \bar{h}^0)_P \quad (20)$$

$$H_R = \Sigma N_R(\bar{h}_f^0 + \bar{h} - \bar{h}^0)_R \quad (21)$$

$$H^0(T) = (R_u T)(a_1 T^{-2} + a_2 \ln(T)/T + a_3 + a_4 T/2 + a_5 T^2/3 + a_6 T^3/4 + a_7 T^4/5 + b_1/T) \quad (22)$$

where $\bar{h}_f^0$, $\bar{h}$ and $\bar{h}^0$ (J mol^{-1}) are the enthalpy of formation, the sensible enthalpy at the specified state and the sensible enthalpy at the standard reference state respectively. Table 2 shows the coefficients required for calculating thermodynamic properties required for eqn (19)–(22).[36]

Moreover, the first-order reaction rate law is applied to estimate the appropriate residence time for ammonia decomposition. This approach is justified as the system operates under atmospheric pressure, where first-order kinetics typically provide a reliable approximation (eqn (23) and (24)).[37]

$$CR = 1 - \exp(-k\tau) \quad (23)$$

$$k = k_0 \exp\left(-\frac{E_a}{R_u T}\right) \quad (24)$$

where k is the apparent rate constant (s^{-1}), which is related to temperature through the Arrhenius formula, where E_a (J mol^{-1}) and k_0 (s^{-1}) are the activation energy and pre-exponential factor respectively.

4. Results and discussions

Considering the ammonia decomposition reaction, by removing the unreacted NH_3 after the reactor using the cold trap and water scrubber, only N_2 and H_2 can pass through the H_2 sensor. Therefore, it can be expected that the sensor should show a volumetric percentage of about 75%, so that the proper performance of these removal parts was confirmed at the commissioning tests of this study by passing ammonia at maximum flow rate and reaching to near zero flow after the removal parts. Moreover, due to performing the purge by N_2 before each test, and the residence time of the flow in each of the components especially the cold trap, a specific time was needed for reaching the steady state condition of the sensor which is required to record the amount of flow rate and conversion rates.

Since most experiments began at 600 °C, Fig. 4 illustrates the change in H_2 concentration (vol%) over time for various flow rates, with H_2 levels recorded every 2 seconds. As the flow rate increased, the system reached steady state more quickly due to reduced residence time—approximately 80, 45, and 35 minutes for 100, 200, and 300 SCCM, respectively. Other factors influencing these durations include conversion rate, cold trap handling and precooling, and the purging time prior to testing. For the 50 SCCM tests, an initial high flow rate of 300 SCCM was used to accelerate stabilization of the H_2 sensor.

The placement of the hydrogen sensor after the cold trap resulted in a longer response time, especially at low flow rates, as the sensor required more time to stabilize and display the H_2 concentration in the H_2/N_2 mixture. This delay was primarily due to the volume of intermediate components, such as the cold trap and water scrubber, which slow down gas flow before

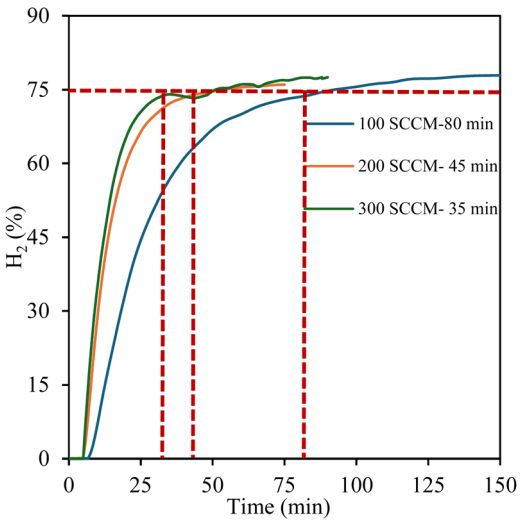

Fig. 4 H_2% variation based on time to reach steady condition.

Table 2 Thermodynamic data coefficients for NH_3, H_2, and N_2 (ref. 36)

	N_2 coefficients (J mol^{-1})	H_2 coefficients (J mol^{-1})	NH_3 coefficients (J mol^{-1})
a_1	2.210×10^4	4.0783×10^4	-7.681×10^4
a_2	-3.818×10^2	-8.009×10^2	1.270×10^3
a_3	6.082	8.214	−3.893
a_4	-8.530×10^{-3}	-1.269×10^{-2}	2.145×10^{-2}
a_5	1.384×10^{-5}	1.753×10^{-5}	-2.183×10^{-5}
a_6	-9.625×10^{-9}	-1.202×10^{-8}	1.317×10^{-8}
a_7	2.519×10^{-12}	3.368×10^{-12}	-3.332×10^{-12}
b_1	7.108×10^2	2.682×10^3	-1.264×10^4
b_2	-1.076×10^1	-3.043×10^1	4.366×10^1

Open Access Article. Published on 28 de maig 2025. Downloaded on 1/2/2026 10:54:36.
This article is licensed under a Creative Commons Attribution-NonCommercial 3.0 Unported Licence.

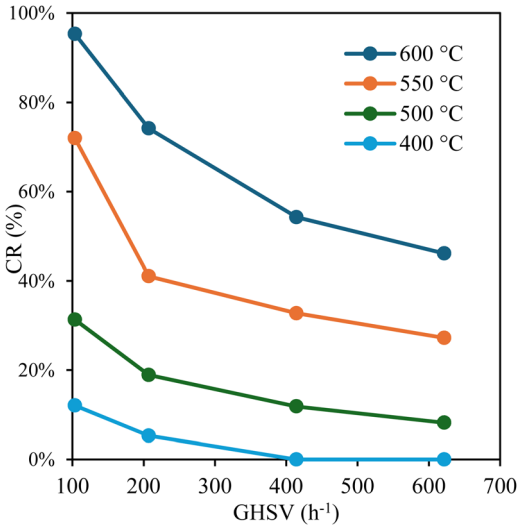

Fig. 5 Conversion rates based on temperature and GHSV of the flows.

reaching the sensor. Additionally, most hydrogen sensors are highly sensitive to the corrosive nature of NH_3, which may affect their accuracy and longevity. To enhance the current setup, an alternative method for monitoring H_2 or NH_3 concentration before ammonia removal could be added. One potential improvement is the use of an acid solution trap coupled with a pH meter.

Fig. 5 illustrates the ammonia conversion rate across different flow rates and temperatures. Higher temperatures significantly improved the ammonia conversion rate across all flow rates.

For example, at GHSV = 104 h^{-1}, the conversion rate increased from 27% at 500 °C to 95% at 600 °C, which is related to the endothermic nature of the ammonia decomposition reaction. Furthermore, lower flow rates at each temperature led to higher conversion rates. For instance, at 550 °C, the conversion rate decreased from approximately 72% at 104 h^{-1} to 27% at 622 h^{-1}. It is worth mentioning that due to the low conversion rates at low temperatures and high flow rates, the results indicate that at 400 °C, only GHSV of 104 h^{-1} and 208 h^{-1} led to

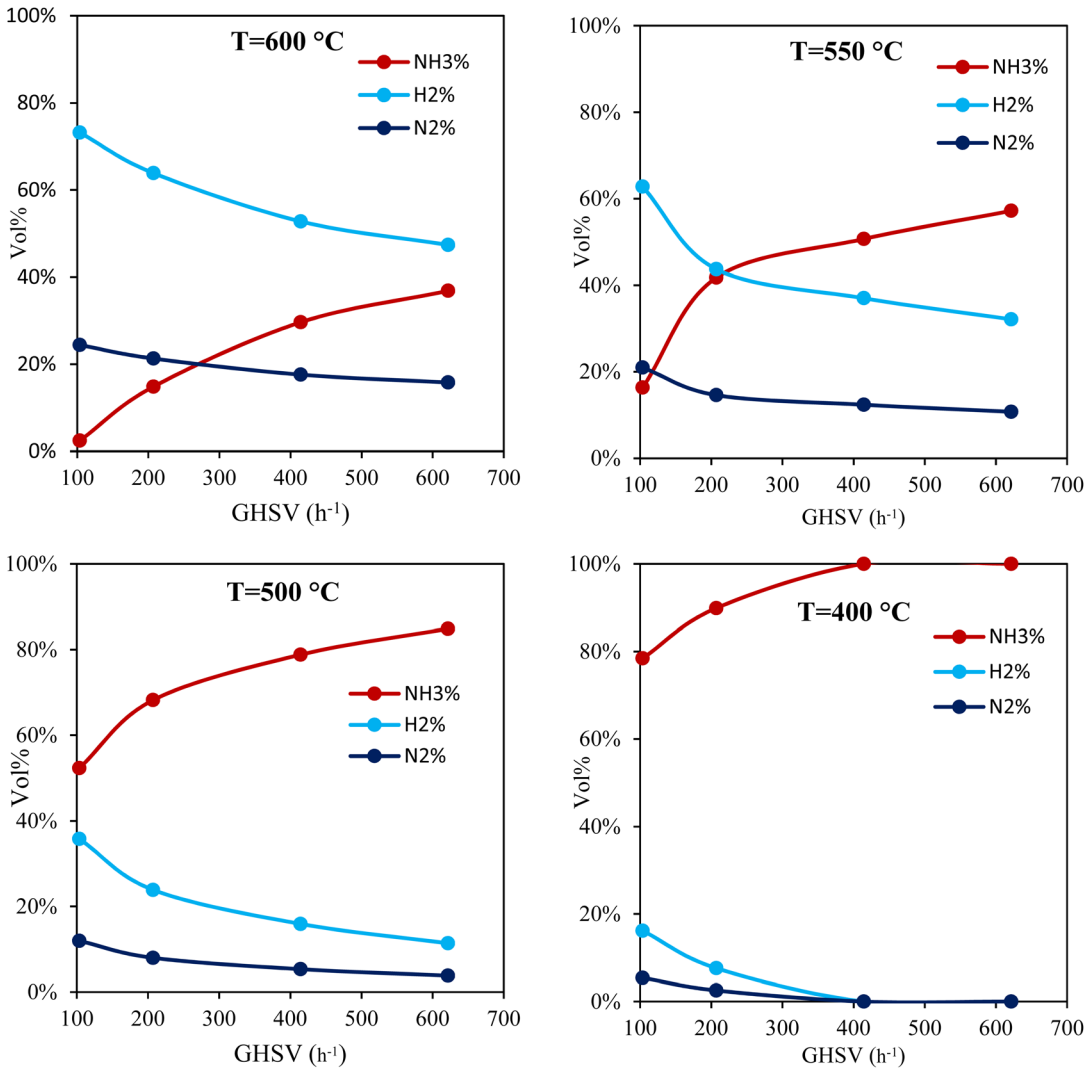

Fig. 6 H_2, N_2 and unreacted NH_3 volumetric percentage based on temperature and flow rates.

 This journal is © The Royal Society of Chemistry 2025

Open Access Article. Published on 28 de maig 2025. Downloaded on 1/2/2026 10:54:36.
This article is licensed under a Creative Commons Attribution-NonCommercial 3.0 Unported Licence.

a conversion rate of about 12% and 5%. For the other flow rates, there was no flow after the cold trap which means that the conversion rate was very close to 0.

Although the catalyst was initially synthesized using 5 wt% Ru/Al_2O_3 powder, the final ruthenium loading on the monolith was lower, approximately 0.1 wt%, due to losses during the wash-coating process. This discrepancy is attributed to poor adhesion and dilution effects during catalyst deposition, resulting in fewer active Ru sites available for ammonia decomposition. As a result, catalytic activity and NH_3 conversion were lower than expected.

Fig. 6 shows the variation of NH_3, H_2 and N_2 volumetric percentage at the outlet of the catalytic system. The results indicate that as GHSV increased, the percentage of H_2 decreased, suggesting that less ammonia is decomposed into hydrogen due to the reduced residence time. This reduction is also accompanied by a decrease in nitrogen concentration. At T = 600 °C and a flow rate of 50 SCCM, the H_2 concentration reached approximately 73%, indicating near-complete ammonia decomposition. However, at 500 °C, this percentage decreased to about 31.7%, with a higher ammonia concentration remaining at the outlet (57.7%). At a conversion rate of 40% (T = 550 °C and GHSV = 200 h^{-1}), the volumetric flow rates of H_2 and unreacted NH_3 became equal. As the conversion rate increased beyond 40%, the H_2 flow rate surpassed that of NH_3. Regarding the minimum flow rate of 50 SCCM and the minimum temperature of 400 °C, H_2 concentration was about 16%.

Fig. 7 illustrates the variation of LHV_{mix}/LHV_{NH3} as a function of GHSV and temperature providing insights into the energy performance of the system. The high ratios reflect the increased energy density of the resulting H_2-rich gas. The ratios decreased significantly as GHSV increased, indicating shorter residence times, which limits the extent of NH_3 conversion. Even at 600 °C, the ratio decreased from 5.2 at 104 h^{-1} to 1.7 at 622 h^{-1}, showing the critical role of contact time. The highest

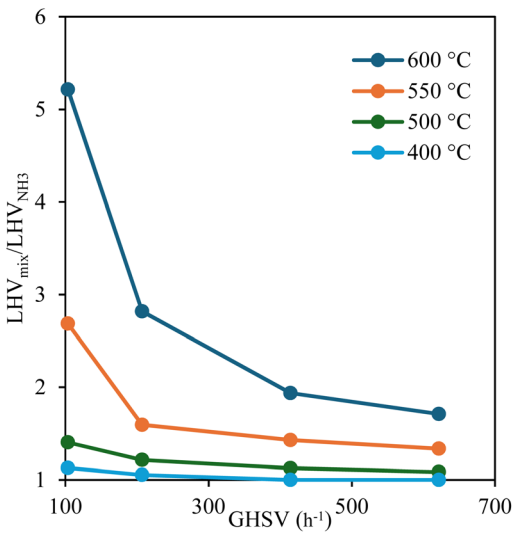

Fig. 7 LHV ratio of the H_2-rich gas to ammonia at different flow rates and temperatures.

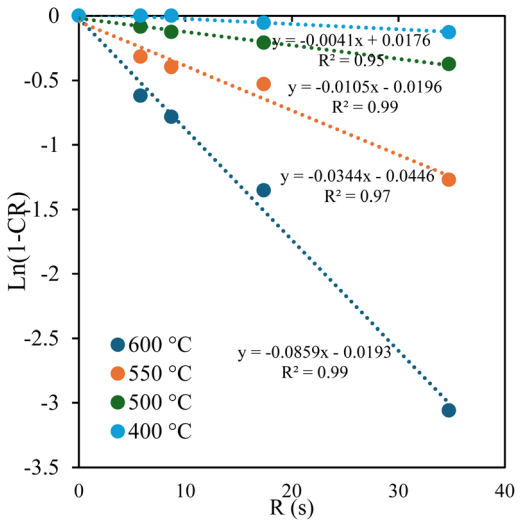

Fig. 8 The effect of residence time on the conversion rate and first-order relation.

ratios were observed at low GHSVs across all temperatures, but at minimum temperature (400 °C), incomplete NH_3 decomposition limited the efficiency of the process so that the LHV ratio at 104 h^{-1} was 1.13.

Therefore, for applications requiring lower temperatures, to enhance the catalytic reactor performance, some of the improvements can be implemented including optimizing catalyst loading by increasing metal dispersion, using promoters such as La and Gd to improve the stability and NH_3 adsorption, incorporating bimetallic Ru-based catalysts such as Ru–Ni, and optimizing reactor volume.

To produce a HRF with an LHV comparable to diesel (approximately 40 MJ kg^{-1}), an ammonia decomposition conversion rate of around 60% is recommended.[16] Moreover, by applying kinetic analysis using eqn (22), Fig. 8 indicates apparent rate constant based on the temperature and residence time conditions. Therefore, to achieve conversion rates exceeding 60% with this catalytic reactor, the residence time must be increased to 85 s at 500 °C and 225 s at 400 °C. This implies that at a flow rate of 50 SCCM, the reactor volume should be increased to 70 cm^3 and 189 cm^3 for 500 °C and 400 °C, respectively, compared to the current volume of 29 cm^3.

Table 3 Estimation of the proper residence time for a real engine

Engine power (kW)	200
Fuel consumption (g kW^{-1} h^{-1})	205
Diesel LHV (MJ kg^{-1})	42.5
Power by H_2-rich gas (kW)	242
Conversion rate	60%
Ammonia input power (kW)	224
Ammonia gas density (kg m^{-3})	0.68
Inlet ammonia flow rate (m^3 h^{-1})	62.5
Number of catalytic reactors	6
Engine size (m^3)	1.6
Proposed volume for each reactor (m^3)	0.013
Residence time (s)	4.5
GHSV (h^{-1})	800

Open Access Article. Published on 28 de maig 2025. Downloaded on 1/2/2026 10:54:36.
This article is licensed under a Creative Commons Attribution-NonCommercial 3.0 Unported Licence.

These results also confirm that, in practical applications, one of the most effective approaches to achieving higher conversion rates while limiting reactor volume is to use catalytic reactors in parallel, thereby increasing the overall residence time. Moreover, based on the values of k from Fig. 8 at each temperature, E_a and k_0 for the catalytic reactor are calculated 72.5 kJ mol^{-1} and 1400 s^{-1}.

Conventional combustion engines have the potential to be modified to dual-fuel engines using H_2-rich fuel, offering a cost-effective alternative to fuel cells that can be utilized at earlier stages of decarbonization. Moreover, kinetic analysis is valuable for scaling up the catalytic reactor system and setting realistic expectations. For example, considering a 200 kW dual-fuel engine operating on diesel and H_2-rich fuel, where 50% of the input energy is supplied by H_2-rich fuel integrated with 6 parallel reactors, Table 3 summarizes the results related to this estimation so the total inlet flow rate needed for ammonia is calculated at about 60 m^3 h^{-1}.

Fig. 9 illustrates the fraction of input energy across different flow rates and temperatures. The results indicate that as temperature increased, in order to reach a specified conversion rate, the required heating energy increased. For example, to achieve a conversion rate of about 70%, the total heating energy required at 600 °C was 3575 kJ $kg_{NH_3}^{-1}$, while this figure for 550 °C was about 3360 kJ $kg_{NH_3}^{-1}$. Moreover, the maximum ratio of heating energy relative to the total input energy was about 18% at 600 °C. For a practical application such as the above-mentioned engine with an available exhaust gas heat of about 85 kW (considering preventing acid condensation at the exhaust gas outlet), to supply the heating energy required for the ammonia decomposition at 400 °C, for CR = 60% and 100%, only 30 and 45 kW heating power are required respectively. Therefore, integrating an optimized thermal catalytic reactor with dual-fuel engines through waste heat recovery can reduce energy consumption, can enhance NH_3 conversion efficiency with minimal external heating, and can improve safety and operational flexibility by eliminating the need for high-pressure hydrogen storage. It is worth mentioning that in practical applications where liquid ammonia is used as the feedstock, the additional energy demand related to ammonia vaporization could be considered. But, considering the dual-fuel engines and the fact ammonia vaporizes at approximately

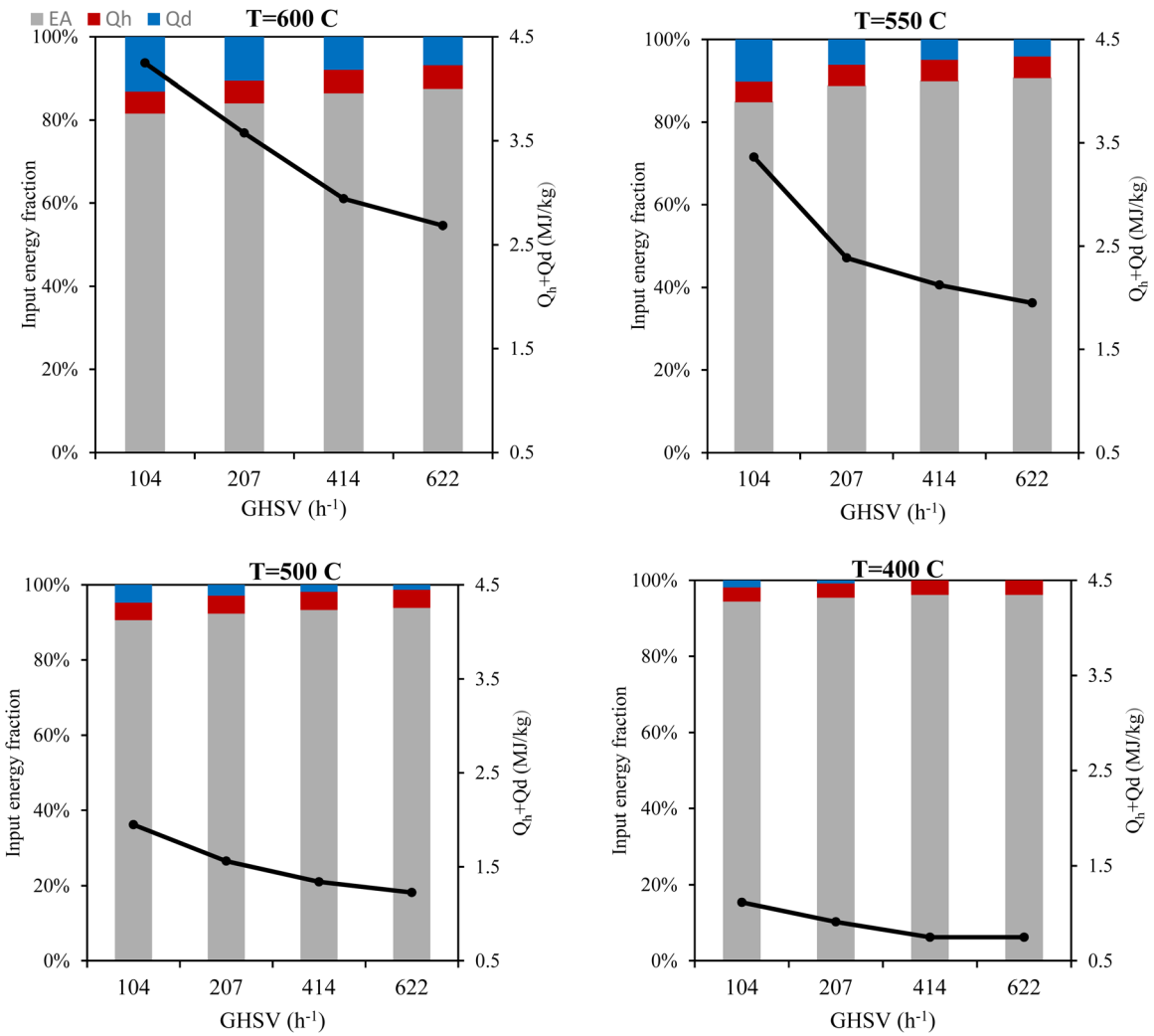

Fig. 9 Input energy fraction and heating energy required for the reaction at different conditions.

 This journal is © The Royal Society of Chemistry 2025

Open Access Article. Published on 28 de maig 2025. Downloaded on 1/2/2026 10:54:36. This article is licensed under a Creative Commons Attribution-NonCommercial 3.0 Unported Licence.

−33 °C, this requirement can typically be met using even low-grade waste heat sources such as engine jacket water (at about 90 °C). Nevertheless, in the absence of such waste heat, the enthalpy of vaporization could become a significant factor.

5. Conclusions

In this study, considering the importance of ammonia decomposition for on-board hydrogen rich gas generation, a non-commercial stainless-steel monolith-based Ru/Al_2O_3 catalyst was experimentally investigated for different ammonia GHSV and operating temperature by analyzing factors such as steady-state time, conversion rate, H_2-rich gas heating value, and required thermal energy. Moreover, the first-order reaction rate law was applied to estimate the appropriate residence time for thermal ammonia decomposition, while feasibility assessments were conducted for a real-scale dual-fuel engine application.

The results indicated that the steady-state time was influenced by factors such as GHSV and conversion rate under different conditions. Higher temperatures notably enhanced ammonia conversion across all GHSVs, consistent with the endothermic nature of ammonia decomposition. Conversely, lower flow rates resulted in higher conversion rates due to increased residence time, with the maximum conversion observed at 600 °C and GHSV = 104 h^{-1}. The actual amount of Ru available on the monolith surface was insufficient to achieve high NH_3 conversion rates at lower temperatures so that the maximum conversion rate at 400 °C was about 12%. This discrepancy highlights the need for improved catalyst deposition techniques to achieve higher active metal dispersion and better adhesion to the monolith structure.

Kinetic estimations illustrated that achieving conversion rates above 50% with this catalytic reactor required increasing the residence time to 85 s at 500 °C. Additionally, to supply 50% of the input energy for a 200 kW dual-fuel engine using hydrogen-rich gas, a 60% conversion rate necessitated limiting the residence time to approximately 4.5 s, corresponding to a GHSV of about 800 h^{-1}. Furthermore, supplying the required thermal energy for ammonia decomposition at 400 °C at a 60% conversion rate would utilize 37% of the available exhaust energy of the dual-fuel engine, demonstrating the feasibility of integrating waste heat recovery with the optimized structured thermo-catalytic reactors.

Therefore, for practical applications operating at lower temperatures, improving catalytic reactor performance can be achieved through different enhancements. These include optimizing catalyst loading by increasing metal dispersion, incorporating promoters like La to enhance stability and ammonia adsorption, utilizing bimetallic Ru-based catalysts such as Ru–Ni, optimizing reactor volume, and implementing a parallel reactor configuration to improve overall efficiency.

Data availability

The data supporting this article have been included as part of the ESI.†

Author contributions

Payam Shafie: conceptualization, methodology, investigation, analysis, writing – original draft, Marie Mottoul: supervision, analysis, review & editing, Alain Dechamplain: conceptualization, supervision, analysis, review & editing, Julien Lepine: conceptualization, supervision, analysis, review & editing.

Conflicts of interest

The authors declare that they have no conflicts of interest.

Acknowledgements

The project was financed by Chantier Davie Canada Inc, as premier shipbuilder in Canada, based on their work in the field of using alternative fuels for marine industry.

References

1 C. Zou, *et al.*, Industrial status, technological progress, challenges, and prospects of hydrogen energy, *Nat. Gas Ind. B*, 2022, **9**(5), 427–447, DOI: 10.1016/j.ngib.2022.04.006.
2 R. Amirante, E. Cassone, E. Distaso and P. Tamburrano, Overview on recent developments in energy storage: Mechanical, electrochemical and hydrogen technologies, *Energy Convers. Manage.*, 2017, **132**, 372–387, DOI: 10.1016/j.enconman.2016.11.046.
3 L. Jiang and X. Fu, An Ammonia–Hydrogen Energy Roadmap for Carbon Neutrality: Opportunity and Challenges in China, *Engineering*, 2021, **7**(12), 1688–1691, DOI: 10.1016/j.eng.2021.11.004.
4 J. Martin, A. Neumann and A. Ødegård, Renewable hydrogen and synthetic fuels versus fossil fuels for trucking, shipping and aviation: A holistic cost model, *Renewable Sustainable Energy Rev.*, 2023, **186**, 113637, DOI: 10.1016/j.rser.2023.113637.
5 P. Shafie, A. DeChamplain and J. Lepine, Thermal Ammonia Decomposition for Hydrogen-Rich Fuel Production and the Role of Waste Heat Recovery, *Int. J. Energy Res.*, 2024, **2024**(1), DOI: 10.1155/2024/9534752.
6 R. Lan, J. T. S. Irvine and S. Tao, Ammonia and related chemicals as potential indirect hydrogen storage materials, *Int. J. Hydrogen Energy*, 2012, **37**(2), 1482–1494, DOI: 10.1016/j.ijhydene.2011.10.004.
7 Production capacity of ammonia worldwide from 2018 to 2022, with a forecast for 2026 and 2030, Accessed: Jul. 13, 2023. [Online], Available: https://www.statista.com/statistics/1065865/ammonia-production-capacity-globally/.
8 C. Smith, A. K. Hill and L. Torrente-Murciano, Current and future role of Haber–Bosch ammonia in a carbon-free energy landscape, *Energy Environ. Sci.*, 2020, **13**(2), 331–344, DOI: 10.1039/C9EE02873K.
9 S. Sittichompoo, *et al.*, Exhaust energy recovery via catalytic ammonia decomposition to hydrogen for low carbon clean vehicles, *Fuel*, 2021, **285**, 119111, DOI: 10.1016/j.fuel.2020.119111.

Open Access Article. Published on 28 de maig 2025. Downloaded on 1/2/2026 10:54:36.
This article is licensed under a Creative Commons Attribution-NonCommercial 3.0 Unported Licence.

10 W. Wang, J. M. Herreros, A. Tsolakis and A. P. E. York, Ammonia as hydrogen carrier for transportation; Investigation of the ammonia exhaust gas fuel reforming, *Int. J. Hydrogen Energy*, 2013, **38**(23), 9907–9917, DOI: 10.1016/j.ijhydene.2013.05.144.
11 V. Alagharu, S. Palanki and K. N. West, Analysis of ammonia decomposition reactor to generate hydrogen for fuel cell applications, *J. Power Sources*, 2010, **195**(3), 829–833, DOI: 10.1016/j.jpowsour.2009.08.024.
12 POSCO Holdings, Growth Vision of POSCO Group and Growth Strategy of Seven Major Core Businesses, https://newsroom.posco.com/en/growth-vision-of-poscogroup-and-growth-strategy-of-seven-major-core-businesses/, accessed 25 March 2023.
13 https://www.investcanada.ca/news/why-canada-leader-ammonia-fuel-future.
14 I. Lucentini, A. Casanovas, and J. Llorca, "Catalytic ammonia decomposition for hydrogen production on Ni, Ru and Ni-Ru supported on CeO 2.".
15 C. Ratnasamy and J. P. Wagner, Water Gas Shift Catalysis, *Catal. Rev.*, 2009, **51**(3), 325–440, DOI: 10.1080/01614940903048661.
16 P. Shafie, A. Dechamplain and J. Lepine, Theoretical investigation of hydrogen-rich fuel production through ammonia decomposition, *Open Chem.*, 2024, **22**(1), DOI: 10.1515/chem-2024-0020.
17 T. A. Le, Q. C. Do, Y. Kim, T.-W. Kim and H.-J. Chae, A review on the recent developments of ruthenium and nickel catalysts for COx-free H2 generation by ammonia decomposition, *Korean J. Chem. Eng.*, 2021, **38**(6), 1087–1103, DOI: 10.1007/s11814-021-0767-7.
18 S.-F. Yin, Q.-H. Zhang, B.-Q. Xu, W.-X. Zhu, C.-F. Ng and C.-T. Au, Investigation on the catalysis of COx-free hydrogen generation from ammonia, *J. Catal.*, 2004, **224**(2), 384–396, DOI: 10.1016/j.jcat.2004.03.008.
19 T. E. Bell and L. Torrente-Murciano, H2 Production via Ammonia Decomposition Using Non-Noble Metal Catalysts: A Review, *Top. Catal.*, 2016, **59**(15–16), 1438–1457, DOI: 10.1007/s11244-016-0653-4.
20 Z. Zhang, S. Liguori, T. F. Fuerst, J. D. Way and C. A. Wolden, Efficient Ammonia Decomposition in a Catalytic Membrane Reactor to Enable Hydrogen Storage and Utilization, *ACS Sustain. Chem. Eng.*, 2019, **7**(6), 5975–5985, DOI: 10.1021/acssuschemeng.8b06065.
21 K. Okura, K. Miyazaki, H. Muroyama, T. Matsui and K. Eguchi, Ammonia decomposition over Ni catalysts supported on perovskite-type oxides for the on-site generation of hydrogen, *RSC Adv.*, 2018, **8**(56), 32102–32110, DOI: 10.1039/C8RA06100A.
22 R.-Y. Chein, Y.-C. Chen, C.-S. Chang and J. N. Chung, Numerical modeling of hydrogen production from ammonia decomposition for fuel cell applications, *Int. J. Hydrogen Energy*, 2010, **35**(2), 589–597, DOI: 10.1016/j.ijhydene.2009.10.098.
23 S. Devkota, *et al.*, Process design and optimization of onsite hydrogen production from ammonia: Reactor design, energy saving and NOX control, *Fuel*, 2023, **342**, 127879, DOI: 10.1016/j.fuel.2023.127879.
24 J. Cha, *et al.*, Ammonia as an efficient COX-free hydrogen carrier: Fundamentals and feasibility analyses for fuel cell applications, *Appl. Energy*, 2018, **224**, 194–204, DOI: 10.1016/j.apenergy.2018.04.100.
25 M. Asif, *et al.*, Recent advances in green hydrogen production, storage and commercial-scale use via catalytic ammonia cracking, *Chem. Eng. J.*, 2023, **473**, 145381, DOI: 10.1016/j.cej.2023.145381.
26 S. Chiuta, R. C. Everson, H. W. J. P. Neomagus, P. van der Gryp and D. G. Bessarabov, Reactor technology options for distributed hydrogen generation via ammonia decomposition: A review, *Int. J. Hydrogen Energy*, 2013, **38**(35), 14968–14991, DOI: 10.1016/j.ijhydene.2013.09.067.
27 R. M. Heck, R. J. Farrauto, and S. T. Gulati, *Catalytic Air Pollution Control*. Wiley, 2009, DOI: 10.1002/9781118397749.
28 C. Plana, S. Armenise, A. Monzón and E. García-Bordejé, Ni on alumina-coated cordierite monoliths for in situ generation of CO-free H2 from ammonia, *J. Catal.*, 2010, **275**(2), 228–235, DOI: 10.1016/j.jcat.2010.07.026.
29 K.-W. Gyak, N. K. Vishwakarma, Y.-H. Hwang, J. Kim, H. Yun and D.-P. Kim, 3D-printed monolithic SiCN ceramic microreactors from a photocurable preceramic resin for the high temperature ammonia cracking process, *React. Chem. Eng.*, 2019, **4**(8), 1393–1399, DOI: 10.1039/C9RE00201D.
30 R. Ao, R. Lu, G. Leng, Y. Zhu, F. Yan and Q. Yu, A Review on Numerical Simulation of Hydrogen Production from Ammonia Decomposition, *Energies*, 2023, **16**(2), 921, DOI: 10.3390/en16020921.
31 J. E. Lee, J. Lee, H. Jeong, Y.-K. Park and B.-S. Kim, Catalytic ammonia decomposition to produce hydrogen: A mini-review, *Chem. Eng. J.*, 2023, **475**, 146108, DOI: 10.1016/j.cej.2023.146108.
32 TF55035COMA-1 Lindberg/Blue M Mini-Mite Tube Furnace, https://www.thermofisher.com/order/catalog/product/TF55035A-1.
33 Ammonia, Anhydrous Safety Data Sheet E-4562 according to the Hazardous Products Regulation, [Online], Available: https://www.lindecanada.ca/shop/en/ca/home.
34 S. Sittichompoo, H. Nozari, J. M. Herreros, N. Serhan, J. Silva, A. York, P. Millington and A. Tsolakis, Exhaust energy recovery via catalytic ammonia decomposition to hydrogen for low carbon clean vehicles, *Fuel*, 2021, **285**, 119111, DOI: 10.1016/j.fuel.2020.119111.
35 Y. A. Çengel and M. A. Boles, *Thermodynamics: An Engineering Approach*, McGraw-Hill, 8th edn, 2015.
36 B. J. Mcbride, M. J. Zehe, and S. Gordon, NASA Glenn Coefficients for Calculating Thermodynamic Properties of Individual Species, 2002. [Online]. Available: http://www.sti.nasa.gov.
37 H. Maleki, M. Fulton and V. Bertola, Kinetic assessment of H2 production from NH3 decomposition over CoCeAlO catalyst in a microreactor: Experiments and CFD modelling, *Chem. Eng. J.*, 2021, **411**, 128595, DOI: 10.1016/j.cej.2021.128595.

 This journal is © The Royal Society of Chemistry 2025